



Structure Design of Jointless Cement Concrete Pavement

Zhihua Niu¹^a and Xiaoyu Liu^{2,*}^b

¹PowerChina Northwest Engineering Corporation Limited, No.18 Zhangba Road, Yanta District, Xi'an 710065, China

²School of Civil Engineering, Xi'an University of Architecture and Technology, No. 13 Yanta Road, Beilin District, Xi'an 710055, China

*

Keywords: Jointless Cement Concrete Pavement, Structure Design, ECC, Finite Element Model, Stress Analysis.

Abstract: Joints in cement concrete pavements frequently contribute to decreased ride quality, accelerated pavement deterioration, and complex maintenance procedures. To mitigate these issues, this study proposes the use of engineered cementitious composites (ECC) as connectors at pavement joints, creating a jointless cement concrete pavement (JCCP) system. A finite element model was developed to evaluate the structural performance of JCCP, taking into account variables such as vehicle loading, width and thickness of ECC connector dimensions. The mechanical behavior of the JCCP under combined loading and temperature-induced stresses was analyzed, and the critical load position was identified. The results reveal that the most critical load position occurs directly above the induced crack in the pavement. The integration of ECC connecting elements reduced the maximum tensile stress at the base of the pavement by nearly 50%. Based on these findings, it is recommended to utilize ECC connectors with a width of 30 cm, and a thickness equal to 50% of the pavement slab's thickness.


1 INTRODUCTION


Compared to asphalt pavements, cement concrete pavements have several advantages, including lower construction costs, higher stiffness, longer service life, and better stability (Plati 2019). However, the application of cement concrete pavements in high-class highways has been declining due to the negative impacts of joints, such as poor ride quality, increased susceptibility to pavement distresses, and difficult maintenance. To address these limitations, optimizing the joint design of cement concrete pavements, reducing the number of joints, and even achieving jointless constructions can significantly improve pavement performance and promote the wider adoption of cement concrete pavements in high-class highways.

To mitigate cracking induced by temperature and shrinkage stresses in concrete pavements, equally spaced transverse and longitudinal joints are typically constructed to accommodate these stresses (Das et al., 2020). Joints are critical components of concrete

pavements but are also the weakest points, prone to failures such as slab pumping, faulting, and spalling. Existing research has demonstrated that the majority of distress in concrete pavements is concentrated around joint edges, particularly at the corners where transverse and longitudinal joints intersect. Existing measures to mitigate the adverse effects of joints primarily involve regular cleaning and maintenance of the pavement surface and joints, especially during the early stages of service life. However, these measures can only delay the onset of joint-related distress and do not fundamentally eliminate the negative impacts of joints.

Engineered Cementitious Composites (ECC) exhibit exceptional ductility and toughness, with ultimate tensile strains reaching 3-8%, which is 300-800 times that of ordinary concrete (Li 1993). This superior deformability makes ECC an excellent candidate for accommodating deformations in concrete pavements induced by temperature variations (Arce et al., 2021). Moreover, ECC possesses outstanding crack control capabilities, dispersing single cracks in ordinary concrete into

^a <https://orcid.org/0009-0000-9338-1508>

^b <https://orcid.org/0009-0004-5745-0341>

multiple microcracks with widths less than 100 μm , and exhibiting self-healing properties (Shi et al., 2017). The ultra-high toughness, high tensile strain capacity, and superior crack resistance of ECC enable it to absorb the deformations caused by thermal stresses in concrete pavements (Singh et al., 2019). By undergoing tensile and compressive deformations, ECC can accommodate structural deformations resulting from temperature changes. Additionally, the exceptional ductility and multiple cracking characteristics of ECC effectively inhibit and delay the initiation and propagation of cracks in concrete pavements, thereby prolonging the service life of the entire pavement structure (Ismail et al., 2018). Zhang et al. (Zhang et al., 2017; Zhang et al., 2013) explored the performance of jointless concrete pavements and found that ECC could continue to transmit forces even after cracking. Although a limited number of studies have been conducted on the application of ECC in jointless concrete pavements in China (Cao 2021), specific structural design parameters for ECC have not been clearly established, and corresponding design methods are lacking. This paper develops a finite element model of a jointless concrete pavement structure, considering the effects of loading and temperature stresses, to investigate and analyze the mechanical response of the pavement structure under various ECC connecting segment widths and thicknesses. The objective is to determine the optimal design parameters for ECC connecting segments in jointless concrete pavements and to optimize the design of jointless concrete pavement structures.

2 PAVEMENT STRUCTURE AND MATERIALS

This paper establishes two types of pavement structures: jointed plain concrete pavement (JPCP) and jointless cement concrete pavement (JCCP). Appropriate pavement materials were selected, and ECC were prepared for use in the corresponding pavement structures.

2.1 JPCP

As shown in Figure 1(a), the JPCP structure consists of a subgrade, a base course, and a surface course. As illustrated in Figure 1(b), the surface course is composed of nine $5\text{ m} \times 4\text{ m} \times 0.28\text{ m}$ concrete slabs joined together with a 6 mm joint spacing. The base course consists of a 0.36 m thick cement-stabilized base layer.

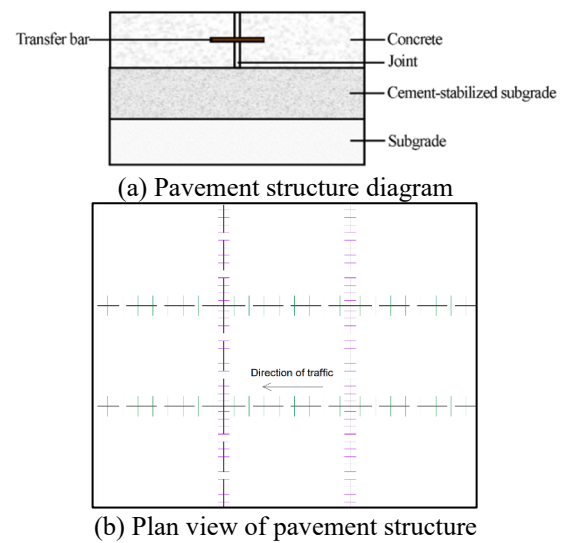


Figure 1: JPCP structure.

2.2 JCCP

As shown in Figure 2 (a), the JCCP structure is developed based on the JPCP structure by replacing the traditional joints with ECC transition zones. An induced crack is set directly below the ECC transition zone, with the transfer bar located at the middle of the induced crack and the anchorage steel bars located at the middle of the interface between the ECC transition zone and the concrete slab. Figure 2 (b) is a plan view of the JCCP structure, where both transverse and longitudinal joints are replaced by ECC transition zones.

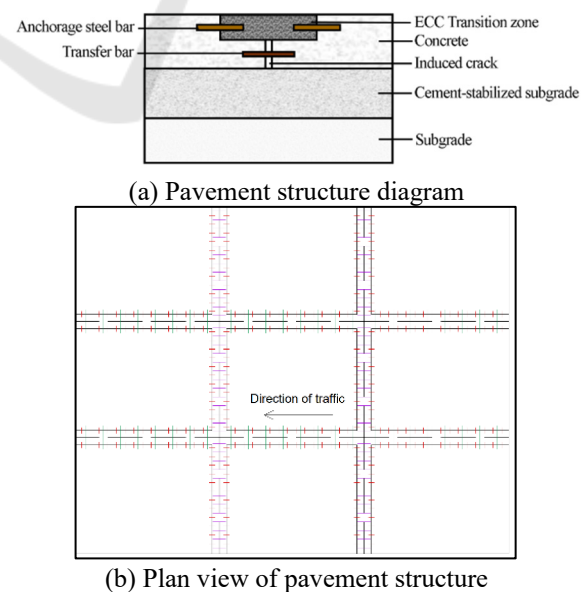


Figure 2: JCCP structure.

2.3 Pavement Materials

C50 concrete was selected as the cement concrete surface layer material for both pavement structures, while ECC material was prepared for the ECC transition zone of the JCCP structure. The raw materials for ECC included cement, fly ash, silica sand, water reducer, and polyethylene (PE) fiber. Four-point bending tests and elastic modulus tests were conducted to determine the flexural strength of C50 and ECC, which were found to be 5.1MPa and 20.0MPa, respectively. The elastic modulus of C50 and ECC were 36100MPa and 29800MPa, respectively, and the subgrade reaction modulus was 60MN/m³. The pavement materials parameters are shown in Table 1.

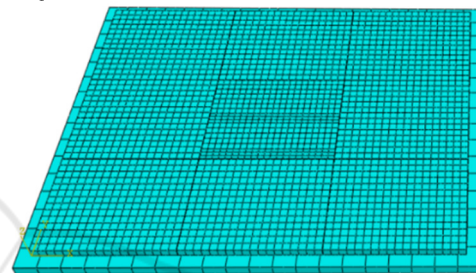
Table 1: Pavement material parameters.

Materials	Flexural strength (MPa)	Elastic modulus (MPa)	Poisson's ratio	Density (kg/m ³)	Thickness (m)
Concrete	5.1	36100	0.15	2800	0.28
ECC Transition zone	20.0	29800	0.15	2000	0.14
Cement-stabilized base	/	1800	0.25	2200	0.36
Transfer and Tie bar Anchorage steel bar	/	200000	0.3	7850	/
Subgrade	Reaction modulus: 60 (MN/m ³)				

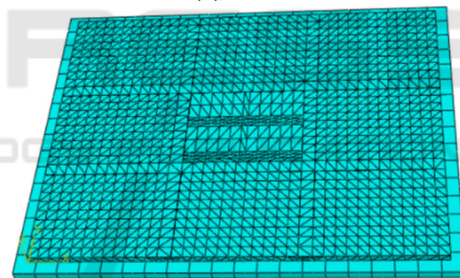
3 FINITE ELEMENT MODEL ESTABLISHMENT AND VERIFICATION

3.1 Establishment and Mechanical Responses Analysis of Two Pavement Models

In this paper, two pavement structure models were established using ABAQUS software to simulate and analyze the mechanical response of the pavement under load and temperature. As shown in Figures 3 (a) and (b), nine concrete slabs were set up in the ABAQUS finite element model.



(a) Model of JPCP



(b) Model of JCCP

Figure 3: Finite element model of the pavement structure.

This study used a typical winter day in Xi'an with a significant temperature gradient as a reference to establish temperature field conditions for the two pavement models (Wu 1992). The temperature field was defined based on the temperature distribution at various depths at the time of the lowest daily temperature. Figure 4 illustrates the temperature distribution at different depths at the moment of the lowest daily temperature.

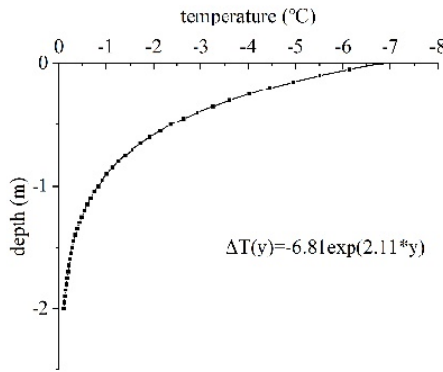


Figure 4: Minimum temperature at various depths in Xi'an.

In this study, a single-axle dual-wheel assembly load was applied, with axle loads of 100kN, 150kN, and 180kN, respectively. These axle loads were converted into rectangular uniformly distributed loads as shown in Figure 5. There were two wheels on each side, with a center-to-center spacing of 0.32m. The contact area of the wheel load was simplified as $0.23\text{m} \times 0.16\text{m}$.



Figure 5: Distribution of vehicle load on the pavement (unit: m).

3.2 Stress Responses in JPCP

Based on the pavement structure and material parameters in Section 2, the load stress and temperature stress of ordinary Portland cement concrete pavement are calculated. First, the stress in the pavement slab under different axle loads was calculated. Since the lower layer is made of cement-stabilized gravel, there is no need to calculate its load stress. Only the load stress of the upper cement slab under the design load is calculated, which is obtained from Equation 1:

$$\sigma_p = \frac{1.45 \times 10^{-3}}{1 + \frac{D_b}{D_c}} r_g^{0.65} h_c^{-2} P^{0.94} \quad (1)$$

where σ_p is the stress due to load, D_b is the flexural rigidity of the lower plate, D_c is the flexural rigidity of the upper plate, r_g is the total relative stiffness radius of the two-layer plate, h_c is the flexural thickness of the upper plate, and P is the design load.

The maximum temperature stress in the concrete pavement slab under the maximum temperature gradient is calculated as shown in Equation 2:

$$\sigma_{t,\max} = \frac{\alpha_c E_c h_c T_g}{2} B_L \quad (2)$$

where α_c is the coefficient of linear thermal expansion of concrete, E_c is the modulus of elasticity of the upper plate, T_g is the maximum temperature gradient, and B_L is the temperature stress coefficient considering both temperature warping stress and internal stress.

Equation 3 gives the calculated temperature fatigue stress at the critical load position of the surface layer.

$$\sigma_{tr} = k_t \sigma_{t,\max} \quad (3)$$

where k_t is defined as the temperature fatigue stress coefficient.

The theoretical calculation results of load stress and temperature stress for JPCP are presented in Table 2.

Table 2: Theoretical calculation results of JPCP stress response (Unit: MPa).

Theoretical Calculation Results of JPCP Stress Response	load stress	100kN	1.501
		150kN	2.198
		180kN	2.609
	temperature stress	thermal fatigue stress	0.306
		maximum thermal warping stress	1.101

3.3 Finite Element Model Verification

A comparison between the finite element simulation results and theoretical calculation results of JPCP under load stress is presented in Table 3. The maximum error between the two is 6.48%. Therefore, the finite element model established in this paper is reasonable and feasible.

Table 3: Comparison of finite element simulation and theoretical calculation results for JPCP.

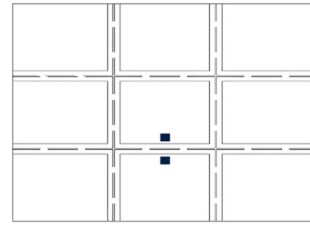
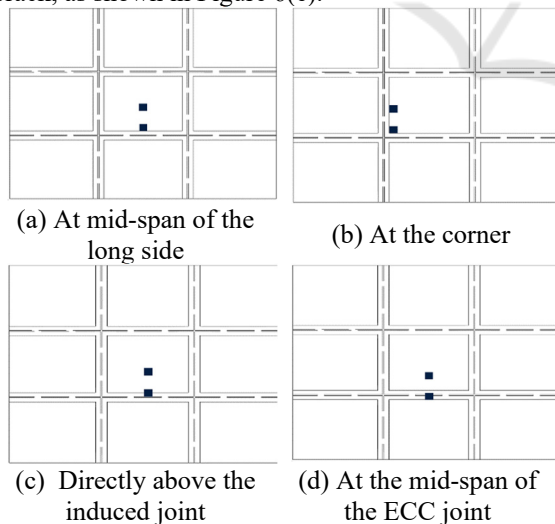
Axle load	Theoretical calculated value (MPa)	Finite element simulation value (MPa)	Error (%)

100kN	1.501	1.490	0.73
150kN	2.198	2.122	3.46
180kN	2.609	2.440	6.48

4 INFLUENCE OF STRUCTURAL DESIGN PARAMETERS OF ECC JOINTS ON MECHANICAL RESPONSE

4.1 Determination of Critical Load Position

The critical load position for JPCP is at the mid-span of the longitudinal joint, according to the design code. However, as a novel pavement structure, the critical load position of JCCP needs to be determined. In this study, a JCCP structure with an ECC joint width of 50 cm and thickness of 14 cm is taken as an example to analyze the stress response of JCCP under loads applied at five different positions. The five load positions are as follows: (a) load at the mid-span of the long side of the concrete slab, as shown in Figure 6(a); (b) load at the corner of the concrete slab, as shown in Figure 6(b); (c) load directly above the induced crack, as shown in Figure 6(c); (d) load at the mid-span of the ECC joint, as shown in Figure 6(d); (e) load on both sides directly above the induced crack, as shown in Figure 6(e).



(e) Both sides directly above the induced crack

Figure 6: Different load positions.

The influence of different load positions on the maximum tensile stress in each structural layer is shown in Table 4 based on finite element simulation results.

Table 4: Maximum tensile stress values in different load positions. (unit: MPa).

Load positions	Cement concrete slab	Base course	ECC joint	Re bar
(a) At the mid-span of the long side of the concrete slab	0.757	0.057	0.456	8.023
(b) At the corner of the concrete slab	0.764	0.060	0.465	8.638
(c) Load directly above the induced crack	0.767	0.063	0.591	14.811
(d) Load at the mid-span of the ECC joint	0.725	0.056	0.516	18.210
(e) Load on both sides directly above the induced crack	0.725	0.045	0.217	7.115

The maximum tensile stress at the bottom of the JCCP surface layer is only about 50% of that of the JPCP. Tensile stresses at the bottom of each layer reach their maximum when the load is applied directly above the center of the induced crack. The maximum tensile stress at the bottom of the surface

layer under this condition is 0.767MPa. Conversely, the minimum tensile stresses in each layer occur when the load is applied on both sides directly above the induced crack. Therefore, the critical load position of the JCCP is determined to be directly above the center of the induced crack.

4.2 Determination of Width of ECC Joint

To investigate the influence of ECC joint width on the stress response of JCCP, the ECC joint widths were varied as 5cm, 10cm, 15cm, 20cm, 30cm, 40cm, 50cm, and 60cm. The upper width of the ordinary concrete section varied accordingly, while the lower part remained constant at 5m×4m. The thickness of the ECC joint was still half of the surface slab. Figure 7 shows the variation of maximum tensile stress at the bottom of the slab for different ECC joint widths.

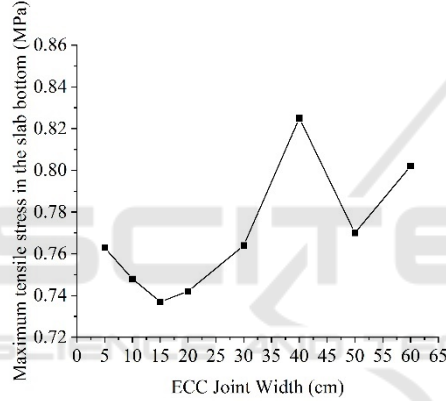


Figure 7: Influence of ECC joint width on maximum tensile stress at the slab bottom.

As shown in Figure 7, the maximum tensile stress at the bottom of the slab initially decreases and then increases with the increase of ECC joint width. The minimum value of 0.737MPa is obtained when the width is 15cm. When the ECC joint width is 40cm, the maximum tensile stress at the bottom of the slab increases abnormally, which is because the first wheel on the left side of the single-axle dual-wheel load in the driving direction acts entirely on the ECC joint at this time, but its stress is 0.825MPa, which is still less than that of JPCP.

In addition, concrete slabs are subjected to temperature and shrinkage deformations. To prevent cracking, joints are usually required in JPCP. For JCCP, ECC has excellent ductility and deformability. It is required that the ECC joint at the joint position can absorb the tensile strain caused by temperature and shrinkage deformation of the slab. Therefore,

when determining the width of the ECC joint, it is necessary to ensure that the ultimate tensile strain of ECC is not less than the required value of the overall tensile strain of the slab. The required value of the overall tensile strain of the slab can be calculated theoretically and is related to temperature and concrete shrinkage deformation, as shown in Equation 4.

$$\epsilon_R = \alpha_T \Delta T + \epsilon_{sh} \quad (4)$$

where ϵ_R is the required tensile strain of the entire pavement slab, α_T is the thermal expansion coefficient of concrete, typically taken as 0.001%/°C, ΔT is the annual temperature difference (about 40°C in Xi'an), and ϵ_{sh} is the concrete shrinkage strain, typically 0.06%. The calculated value of ϵ_R is 0.10%.

The overall strain capacity of the pavement slab in the longitudinal direction under uniaxial tension is given by Equation 5.

$$\epsilon_c = \epsilon_I \left(\frac{L_I}{L} \right) + \epsilon_{II} \left(\frac{L_{II}}{L} \right) \quad (5)$$

where ϵ_I is the ultimate tensile strain of ECC, ϵ_{II} is the strain of concrete under the corresponding axial tensile load, L is the length of the pavement slab, and L_I and L_{II} are the lengths of the ECC and concrete sections, respectively.

Both the ultimate tensile strain and width of the ECC joint can enhance the overall deformation capacity of the slab. For a 5m long slab, a conservative value of 1.5% is adopted for the ultimate tensile strain of the ECC joint, while the strain of concrete under corresponding axial tensile load is obtained from experiments and is taken as 0.01% in this case. Substituting the required strain value obtained from the above equation into the overall deformation capacity, we finally obtain: $L_I = 268.46\text{mm}$, $L_{II} = 4731.54\text{mm}$. Considering the calculation results and a certain safety factor, as well as construction convenience, the width of the ECC joint for a 5.0m long slab is determined to be 300mm.

4.3 Determination of Thickness of ECC Joint

To investigate the influence of ECC joint thickness on the stress response of JCCP, the ECC joint thickness was varied as 25%, 40%, 50%, 60%, and 75% of the pavement slab thickness. Figure 8 illustrates the variation of maximum tensile stress at

the bottom of the slab for different ECC joint thicknesses.

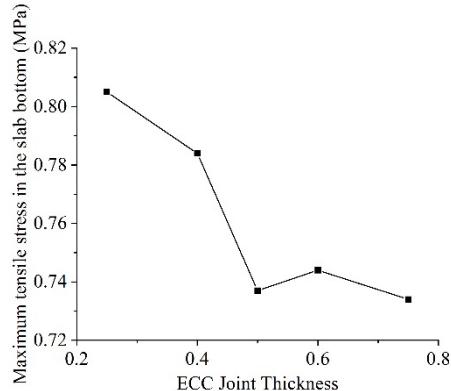


Figure 8: Influence of ECC joint thickness on maximum tensile stress at the slab bottom.

As shown in the Figure 8, the maximum tensile stress at the bottom of the slab decreases with the increase in the thickness ratio of the ECC joint. After the thickness ratio reaches 50%, the change in the maximum tensile stress at the bottom of the slab becomes insignificant. The selection of ECC joint thickness should also consider the diameter of the anchor bars, force transfer bars, and tension bars, as well as the concrete cover thickness. For the JCCP structure proposed in this paper, it is recommended to select an ECC joint thickness ratio of 50%.

5 CONCLUSIONS

In this study, a jointless concrete pavement with an engineered cementitious composite (JCCP) was designed, and a finite element model of the JCCP structure was established. Considering the effects of load stress and temperature stress, the influence of vehicle load, ECC joint width, and thickness on the mechanical response of JCCP was investigated and analyzed, and the JCCP structure was optimized.

- (1) Compared with JPCP, the maximum tensile stress at the bottom of the JCCP surface layer is only about 50% of that of JPCP, indicating that JCCP can effectively reduce the stress in the concrete slab.
- (2) By comparing the stress responses of JCCP under different load positions, it was determined that the critical load position of JCCP is the middle of the slab directly above the induced crack.
- (3) For the JCCP structure proposed in this paper, it is recommended that the width of the ECC joint

be 30 cm, and the thickness be 50% of the pavement slab thickness.

ACKNOWLEDGMENTS

This research was funded by Scientific Research Program Funded by Education Department of Shaanxi Provincial Government (Program No.23JC046)

REFERENCES

- Plati, C., 2019. Sustainability factors in pavement materials, design, and preservation strategies: A literature review. *Construction and Building Materials* 211, 539-555.
- Das, A., Bhuyan, M.R., Khattak, M.J., Zhang, Q., 2020. Mitigating reflective cracking in composite pavements through the use of a ductile concrete interlayer. *Construction and Building Materials*, 259, 120383.
- Li, V.C., Stang, H., Krenchel, H., 1993. Micromechanics of crack bridging in fibre-reinforced concrete. *Materials and Structures*, 26, 486-494.
- Arce, G.A., Noorvand, H., Hassan, M.M., Rupnow, T., Dhakal, N., 2021. Feasibility of low fiber content PVA-ECC for jointless pavement application. *Composites: Part B*, 50, 224-231.
- Shi, T., Leung, C.K.Y., 2017. An effective discrete model for strain hardening cementitious composites: Model and concept. *Computers and Structures*, 185, 27-46.
- Singh, M., Saini, B., Chalak, H.D., 2019. Performance and composition analysis of engineered cementitious composite (ECC) – A review. *Journal of Building Engineering*, 26, 100851.
- Ismail, M.K., Hassan, A.A.A., Lachemi, M., 2018. Effect of Fiber Type on Impact and Abrasion Resistance of Engineered Cementitious Composite. *Aci Materials Journal*, 115(6), 957-968.
- Zhang, J., Chen, Q., Wang, Z., Chen, C., Guo, Z., Fu, Y., 2017. Design and construction of jointless concrete pavement. *Journal of Harbin Institute of Technology*, 49(3), 68-73.
- Zhang, J., Wang, Z., Ju, X., 2013. Application of ductile fiber reinforced cementitious composite in jointless concrete pavements. *Composites: Part B*, 50, 224-231.
- Cao, W., 2021. Application of ECC Materials in Rigid-flexible Composite Long-life Pavement. *Journal of Municipal Technology*, 39(9), 180-183.
- Wu, G., 1992. The Analysis of Pavement Temperature Field of Multi-layer System. *China Journal of Highway and Transport*, 5(5), 17-25.